Master-equation theory of multimode semiconductor lasers. II. Injection locking

A. Eschmann
Physics Department, University of Waikato, Hamilton, New Zealand

C. W. Gardiner
Physics Department, Victoria University of Wellington, Wellington, New Zealand

(Received 5 March 1996)

The master-equation theory for multimode semiconductor lasers [A. Eschmann and C. W. Gardiner, Phys. Rev. A **54**, 760 (1996)] is adapted to treat the case of an injection-locked laser. Both the intensity noise and the phase noise of the system are examined. A decrease in the total intensity noise and in the intensity noises of the individual modes is found for increasing injection power, provided the injection signal does not dominate the entire system. A regime is found in which a reduction of the intensity noise below the shot noise level is obtained which is not single-mode squeezing, but which is due to anticorrelations between the individual modes, and a further regime in which true single-mode squeezing exists is also found. The phase noise is found to decrease with increasing injection strength, in other words as phase locking occurs. [S1050-2947(96)05409-1]

PACS number(s): 42.50.Dv, 42.50.Lc, 42.55.Px

I. INTRODUCTION

The experiment of Marin *et al.* [1] examined intensity squeezing in three different semiconductor laser systems, a free-running laser, an injection-locked laser, and an external grating laser. It was found that the type of squeezing which occured was different for each laser system, and it was thus concluded that the type of squeezing obtainable depended on the degree of sidemode rejection of a system.

In a previous paper [2] (which we refer to here as I), we considered the free-running and external grating laser theoretically, using a master-equation description for the multimode semiconductor laser. We found results which agreed with those of Marin *et al.*; for the free-running case, there is no squeezing, and for the external grating case, single-mode squeezing is obtained.

In this paper we focus our attention on the other situation considered by Marin *et al.* of injection locking, which completes a comparison with their work. In this case Marin *et al.* found that although there was squeezing of the total intensity noise, the individual mode noises were unsqueezed. Thus squeezing in the sense of single-mode squeezing is not obtained, but squeezing of the total intensity noise arises as the result of anticorrelated fluctuations of the individual modes in the semiconductor. In addition to examining this intensity noise theoretically, we also examine the phase noise of the system, to see whether a reduction in noise occurs as locking takes place.

In Sec. II we introduce the additional terms and equation which must be included in a description of injection locking. In Sec. III the linearized equations are given, which lead to the drift and diffusion matrices used in calculating the spectrum. In Sec. IV we discuss how the steady-state solutions are obtained, and in Sec. V give a detailed description of the results obtained.

II. INCLUSION OF INJECTION LOCKING

Injection locking involves feeding a stable coherent signal into the system. This serves the purpose of locking the frequency of the dominant mode of the system to that of the injected signal, the effect of which is to stabilize the system with regard to fluctuations in the frequency.

Mathematically this process is written in terms of a Hamiltonian which introduces a coupling between the dominant mode and the injected signal.

$$H_{\mathrm{inj}} = i\hbar(b_1^\dagger \epsilon - b_1 \epsilon^*), \tag{1}$$

where $|\epsilon|$ is proportional to the amplitude of the coherent injected signal, and b_1 is the annihilation operator for a photon in the dominant mode. Using standard input-output theory arguments, the injected power in units of photons per second can be found in terms of $|\epsilon|$ to be $4|\epsilon|^2/\kappa$. All other Hamiltonian contributions are the same as in Sec. II of I, and the reader is referred there and to Sec. II of the single-mode treatment [3] for these terms.

Standard techniques can be used to write down the injection-locking contribution to the master equation.

$$\left.\frac{\partial \rho_0(\underline{n})}{\partial t}\right|_{\mathrm{inj}} = \frac{-i}{\hbar}[H_{\mathrm{inj}}, \rho] = b_1^\dagger \epsilon \rho - b_1 \epsilon^* \rho - \rho b_1^\dagger \epsilon + \rho b_1 \epsilon^*. \tag{2}$$

The remaining master-equation contributions are given in Sec. III of [2] and Eq. (53) of [3]. Using operator correspondences [4] to convert to the positive P representation, the contribution to the Fokker-Planck equation obtained due to injection locking is

$$\left.\frac{\partial P(\mathbf{X})}{\partial t}\right|_{\mathrm{inj}} = \left[-\frac{\partial}{\partial \beta_1}\epsilon - \frac{\partial}{\partial \beta_1^*}\epsilon^* \right] P(\mathbf{X}), \tag{3}$$

where $\mathbf{X}$ is defined in Eq. (14) of I. This contribution leads to additional terms in two of the stochastic differential equations (SDE's), Eqs. (C1)–(C6) of I. For clarity and completeness, these altered equations [Eqs. (C5) and (C6) of I] are given here in full.

$$d(\beta_1)=\left\{\sum_j\ [G^*_{j1}(\underline{n})\beta_j-F^*_{j1}(\underline{n})\beta_j]-\frac{\kappa_1\beta_1}{2}-i\Delta_1\beta_1+\widetilde{G}^*_{11}(\underline{n})\beta_1-\widetilde{F}^*_{11}(\underline{n})\beta_1+\epsilon\right\}dt$$

$$-\sum_j\ v_{1j}d\eta_j+\sqrt{\kappa_1 N_1}d\Xi_1-\widetilde{v}_{11}d\widetilde{\eta}, \tag{4}$$

$$d(\beta^*_1)=\left\{\sum_j\ [G_{1j}(\underline{n})\beta^*_j-F_{1j}(\underline{n})\beta^*_j]-\frac{\kappa_1\beta^*_1}{2}+i\Delta_1\beta^*_1+\widetilde{G}_{11}(\underline{n})\beta^*_1-\widetilde{F}_{11}(\underline{n})\beta^*_1+\epsilon^*\right\}dt$$

$$-\sum_j\ v^*_{1j}d\eta^*_j+\sqrt{\kappa_1 N_1}d\Xi^*_1-\widetilde{v}^*_{11}d\widetilde{\eta}^*, \tag{5}$$

where all symbols have the same definitions as in I. Since we wish to calculate the photon number fluctuations, we need a SDE for the central mode photon number, $m_1=\beta^*_1\beta_1$, and such an expression can be obtained from Eqs. (4) and (5) using Ito calculus.

$$d(m_1)=\left\{\sum_j\ [G^*_{j1}(\underline{n})\beta^*_1\beta_j-F^*_{j1}(\underline{n})\beta^*_1\beta_j]+\sum_j\ [G_{1j}(\underline{n})\beta^*_j\beta_1-F_{1j}(\underline{n})\beta^*_j\beta_1]-\kappa_1 m_1+[\widetilde{G}^*_{11}(\underline{n})+\widetilde{G}_{11}(\underline{n})]m_1\right.$$

$$\left.-[\widetilde{F}^*_{11}(\underline{n})+\widetilde{F}_{11}(\underline{n})]m_1+\beta^*_1\epsilon+\beta_1\epsilon^*\right\}dt-\sum_j\ [\beta^*_1 v_{1j}d\eta_j-\beta_1 v^*_{1j}d\eta^*_j]+\sqrt{\kappa_1 N_1}[\beta^*_1 d\Xi_1+\beta_1 d\Xi^*_1]-\beta^*_1\widetilde{v}_1 1 d\widetilde{\eta}$$

$$-\beta_1\widetilde{v}^*_{11}d\widetilde{\eta}^*+\{2G^r_{11}(\underline{n})+\kappa_1\overline{N_1}+2\widetilde{G}^r_{11}(\underline{n})\}dt. \tag{6}$$

Equation (6) can be simplified somewhat by applying the rotating wave approximation (RWA) as done in Sec. VII of I, and setting the phase of the injected field equal to zero. We obtain

$$d(m_1)=\{2G^r_{11}(\underline{n})(m_1+1)-2F^r_{11}(\underline{n})m_1-\kappa_1 m_1+2\widetilde{G}^r_{11}(\underline{n})(m_1+1)-2\widetilde{F}^r_{11}(\underline{n})m_1+\kappa_1\overline{N_1}+|\epsilon|(\beta_1+\beta^*_1)\}dt$$

$$-\sum_j\ [v_{1j}d\eta_j\beta^*_1+v^*_{1j}d\eta^*_j\beta_1]+\sqrt{\kappa_1 N_1}[d\Xi_1\beta^*_1+d\Xi^*_1\beta_1]-(\beta^*_1\widetilde{v}_{11}d\widetilde{\eta}+\beta_1\widetilde{v}^*_{11}d\widetilde{\eta}^*). \tag{7}$$

The remaining equations describing the system are unaltered by the presence of injection-locking and so are not repeated here. The reader is referred to Eqs. (C31)–(C35) of I for these. We can see that the system of equations for the injection-locked system is now no longer closed, since Eq. (7) couples to the field amplitudes β_1 and β^*_1. A closed system can be retained, however, at the expense of introducing a further variable to our system,

$$\beta_{1,+}=\beta_1+\beta^*_1. \tag{8}$$

The variable $\beta_{1,+}$ has the Ito SDE

$$d(\beta_{1,+})=\left\{\sum_j\ [G^*_{j1}(\underline{n})\beta_j+G_{1j}(\underline{n})\beta^*_j-F^*_{j1}(\underline{n})\beta_j-F_{1j}(\underline{n})\beta^*_j]-\frac{\kappa_1}{2}\beta_{1,+}+\beta_{1,+}\widetilde{G}^r_{11}(\underline{n})+\beta_{1,-}\widetilde{G}^i_{11}(\underline{n})-\beta_{1,+}\widetilde{F}^r_{11}(\underline{n})\right.$$

$$\left.-\beta_{1,-}\widetilde{F}^i_{11}(\underline{n})+\epsilon+\epsilon^*\right\}dt-\sum_j\ [v_{1j}d\eta_j+v^*_{1j}d\eta^*_j]+\sqrt{\kappa_1 N_1}[d\Xi_1+d\Xi^*_1]-\widetilde{v}_{11}d\widetilde{\eta}-\widetilde{v}^*_{11}d\widetilde{\eta}^*, \tag{9}$$

where $\beta_{1,-}=-i(\beta_1-\beta^*_1)$.

Making the same approximations as those made in arriving at Eq. (7), and assuming that the imaginary part of G_{lj} and F_{lj} is much less than the real part (this amounts to assuming that the dephasing time is much less than the inverse of the frequency separation between states in the conduction and valence bands, and as such is a realistic assumption), the new variable $\beta_{1,-}$ appearing in the above equation can be eliminated, and the above expression can be simplified to

$$d(\beta_{1,+})=\left\{G^r_{11}(\underline{n})\beta_{1,+}-F^r_{11}(\underline{n})\beta_{1,+}-\frac{\kappa_1}{2}\beta_{1,+}+\beta_{1,+}\widetilde{G}^r_{11}(\underline{n})-\beta_{1,+}\widetilde{F}^r_{11}(\underline{n})+2|\epsilon|\right\}dt-\sum_j\ [v_{1j}d\eta_j+v^*_{1j}d\eta^*_j]$$

$$+\sqrt{\kappa_1 N_1}(d\Xi_1+d\Xi_1^*)-\tilde{v}_{11}d\tilde{\eta}-\tilde{v}_{11}^*d\tilde{\eta}^*, \tag{10}$$

which couples only to $\beta_{1,+}$, and thus a closed system is recovered.

The phase noise of the system is also worth calculating, since it would be interesting to see whether this decreases as the injection strength is increased, and phase locking begins to occur. The easiest correlation to measure the spectrum of, in order to gain information about the phase noise is the $\langle\beta_{1,-}(t)\beta_{1,-}(0)\rangle$ correlation. Since $\beta_{1,-}$ is proportional to the sine of the phase, a reduction in the noise of $\beta_{1,-}$ translates directly into a reduction in the noise of the phase. This is not the case for the variable $\beta_{1,+}$, which is proportional to the cosine of the phase, and hence the phase noise would increase for decreasing noise in $\beta_{1,+}$. Hence, in order to consider the phase noise, we include the SDE for $\beta_{1,-}$ in our system.

The equation of motion for $\beta_{1,-}=-i(\beta_1-\beta_1^*)$ can be written down from Eqs. (5) and (6).

$$d(\beta_{1,-})=\left\{\sum_j\ [-iG_{j1}^*(\underline{n})\beta_j+iG_{1j}(\underline{n})\beta_j^*+iF_{j1}^*(\underline{n})\beta_j-iF_{1j}(\underline{n})\beta_j^*]-\frac{\kappa_1}{2}\beta_{1,-}+i\beta_{1,+}\tilde{G}_{11}^i(\underline{n})+\beta_{1,-}\tilde{G}_{11}^r(\underline{n})-i\beta_{1,+}\tilde{F}_{11}^i(\underline{n})\right.$$
$$\left.-\beta_{1,-}\tilde{F}_{11}^r(\underline{n})-i(\epsilon-\epsilon^*)\right\}dt+i\sum_j\ [v_{1j}d\eta_j-v_{1j}^*d\eta_j^*]-i\sqrt{\kappa_1 N_1}[d\Xi_1-d\Xi_1^*]+i(\tilde{v}_{11}d\tilde{\eta}+\tilde{v}_{11}^*d\tilde{\eta}^*). \tag{11}$$

Making the RWA, setting the phase of the injected field to zero, and assuming that the imaginary parts of the F_{ij} and G_{ij} terms are much less than the real parts, the above expression simplifies to

$$d(\beta_{1,-})=\left\{G_{11}^r(\underline{n})\beta_{1,-}-F_{11}^r(\underline{n})\beta_{1,-}-\frac{\kappa_1}{2}\beta_{1,-}+\beta_{1,-}\tilde{G}_{11}^r(\underline{n})-\beta_{1,-}\tilde{F}_{11}^r(\underline{n})\right\}dt+i\left(\sum_j\ v_{1j}d\eta_j-v_{1j}^*d\eta_j^*\right)$$
$$-i\sqrt{\kappa_1 N_1}(d\Xi_1-d\Xi_1^*)+i(\tilde{v}_{11}d\tilde{\eta}+\tilde{v}_{11}^*d\tilde{\eta}^*). \tag{12}$$

III. LINEARIZED EQUATIONS

Calculation of the spectrum requires use of the drift and diffusion matrices of the system of equations linearized about their steady-state values. These linearized equations are

$$d\mathbf{z}=-\mathcal{F}(\mathbf{Z}_0)\mathbf{z}(t)dt+\mathcal{G}(\mathbf{Z}_0)d\mathbf{W}(t), \tag{13}$$

where

$$\mathbf{z}=\begin{pmatrix} n_e \\ n_h \\ \tilde{n}_e \\ \tilde{n}_h \\ \beta_{1,+} \\ \beta_{1,-} \\ m_1 \\ m_2 \\ m_3 \end{pmatrix}, \tag{14}$$

and the following definitions,

$$r_j=2a_{jj}(m_j^0+1), \tag{15}$$

$$s_{jj}=2a_{jj}(N^2-n_e n_h), \tag{16}$$

$$\tilde{r}_1=2\tilde{a}_{11}(m_1^0+1), \tag{17}$$

$$\tilde{s}_{11}=2\tilde{a}_{11}(\tilde{N}^2-\tilde{n}_e\tilde{n}_h), \tag{18}$$

and

$$t(m_j^0)=2m_j^0 a_{jj}n_e^0 n_h^0, \tag{19}$$

$$u(m_j^0)=t(m_j^0+1)+2m_j^0 a_{jj}N^2+dn_e^0 n_h^0, \tag{20}$$

$$\tilde{t}(m_1^0)=2m_1^0\tilde{a}_{11}\tilde{n}_e^0\tilde{n}_h^0, \tag{21}$$

$$\tilde{u}(m_1^0)=\tilde{t}(m_1^0+1)+2m_1^0\tilde{a}_{11}\tilde{N}^2+\tilde{d}\tilde{n}_e^0\tilde{n}_h^0, \tag{22}$$

are used in the matrices

$\mathcal{F}(\mathbf{Z}_0)$

$$= \begin{pmatrix}
\sum_j (r_j+d)n_h^0 + \alpha_e & \sum_j (r_j+d)n_e^0 + \beta_e & 0 & 0 & 0 & 0 & -s_{11} & -s_{22} & -s_{33} \\
\sum_j (r_j+d)n_h^0 + \beta_h & \sum_j (r_j+d)n_e^0 + \alpha_h & 0 & 0 & 0 & 0 & -s_{11} & -s_{22} & -s_{33} \\
0 & 0 & (\tilde{r}_1+\tilde{d})\tilde{n}_h^0 & (\tilde{r}_1+\tilde{d})\tilde{n}_e^0 & 0 & 0 & -\tilde{s}_{11} & 0 & 0 \\
0 & 0 & (\tilde{r}_1+\tilde{d})\tilde{n}_h^0 & (\tilde{r}_1+\tilde{d})\tilde{n}_e^0 & 0 & 0 & -\tilde{s}_{11} & 0 & 0 \\
-a_{11}\beta_{1,+}^0 n_h^0 & -a_{11}\beta_{1,+}^0 n_e^0 & -\tilde{a}_{11}\beta_{1,+}^0\tilde{n}_h^0 & -\tilde{a}_{11}\beta_{1,+}^0 n_e^0 & \frac{1}{2}(s_{11}+\tilde{s}_{11}+\kappa_1) & 0 & 0 & 0 & 0 \\
-a_{11}\beta_{1,-}^0 n_h^0 & -a_{11}\beta_{1,-}^0 n_e^0 & -\tilde{a}_{11}\beta_{1,-}^0\tilde{n}_h^0 & -\tilde{a}_{11}\beta_{1,-}^0 n_e^0 & 0 & \frac{1}{2}(s_{11}+\tilde{s}_{11}+\kappa_1) & 0 & 0 & 0 \\
-r_1 n_h^0 & -r_1 n_e^0 & -\tilde{r}_1\tilde{n}_h^0 & -\tilde{r}_1\tilde{n}_e^0 & -\epsilon & 0 & s_{11}+\tilde{s}_{11}+\kappa_1 & 0 & 0 \\
-r_2 n_h^0 & -r_2 n_e^0 & 0 & 0 & 0 & 0 & 0 & -s_{22}+\kappa_2 & 0 \\
-r_3 n_h^0 & -r_3 n_h^0 & 0 & 0 & 0 & 0 & 0 & 0 & s_{33}+\kappa_3
\end{pmatrix} \tag{23}$$

and

$$
G(\mathbf{Z}_0) = \begin{pmatrix}
\sum_j u(m_j^0) + D_e & \sum_j u(m_j^0) + D_{eh} & 0 & 0 & -t(\beta_{1,+}^0) & -t(\beta_{1,-}^0) & -2t(m_1^0) & -2t(m_2^0) & -2t(m_3^0) \\
\sum_j u(m_j^0) + D_{he} & \sum_j u(m_j^0) + D_h & 0 & 0 & -t(\beta_{1,+}^0) & -t(\beta_{1,-}^0) & -2t(m_1^0) & -2t(m_2^0) & -2t(m_3^0) \\
0 & 0 & \tilde{u}(m_1^0) + \tilde{D}_e(\underline{n}) & \tilde{u}(m_1^0) + \tilde{D}_{eh}(\underline{n}) & -\tilde{t}(\beta_{1,+}^0) & -\tilde{t}(\beta_{1,-}^0) & -2\tilde{t}(m_1^0) & 0 & 0 \\
0 & 0 & \tilde{u}(m_1^0) + \tilde{D}_{he}(\underline{n}) & \tilde{u}(m_1^0) + \tilde{D}_h(\underline{n}) & -\tilde{t}(\beta_{1,+}^0) & -\tilde{t}(\beta_{1,-}^0) & -2\tilde{t}(m_1^0) & 0 & 0 \\
-t(\beta_{1,+}^0) & -t(\beta_{1,+}^0) & -\tilde{t}(\beta_{1,+}^0) & -\tilde{t}(\beta_{1,+}^0) & 2t(1) + 2\tilde{t}(1) & 0 & t(\beta_{1,+}^0) + \tilde{t}(\beta_{1,+}^0) & 0 & 0 \\
-t(\beta_{1,-}^0) & -t(\beta_{1,-}^0) & -\tilde{t}(\beta_{1,-}^0) & -\tilde{t}(\beta_{1,-}^0) & 0 & 2t(1) + 2\tilde{t}(1) & t(\beta_{1,-}^0) + \tilde{t}(\beta_{1,-}^0) & 0 & 0 \\
-2t(m_1^0) & -2t(m_1^0) & -2\tilde{t}(m_1^0) & -2\tilde{t}(m_1^0) & t(\beta_{1,+}^0) + \tilde{t}(\beta_{1,+}^0) & t(\beta(1,-)^0) + \tilde{t}(\beta_{1,-}^0) & 2t(m_1^0) + 2\tilde{t}(m_1^0) & 0 & 0 \\
-2t(m_2^0) & -2t(m_2^0) & 0 & 0 & 0 & 0 & 0 & 2t(m_2^0) & 0 \\
-2t(m_3^0) & -2t(m_3^0) & 0 & 0 & 0 & 0 & 0 & 0 & 2t(m_3^0)
\end{pmatrix}, \tag{24}
$$

and $\mathbf{Z}_0$ is the vector of steady-state values of $\mathbf{z}$. We have made the same approximations for the $G_{ij}^r(\underline{n})$ and $F_{ij}^r(\underline{n})$ as in I [Eqs. (C23)–(C30)] in the matrices above. In the diffusion matrix we have dropped terms of the form $2G_{k1}^r(\underline{n})\beta_{k,+}$ where $k=2,3$ in the off-diagonal elements where they appear. This can be done for the same reasons as we make the RWA.

Although the variable $\beta_{1,-}$ does not couple to any of the

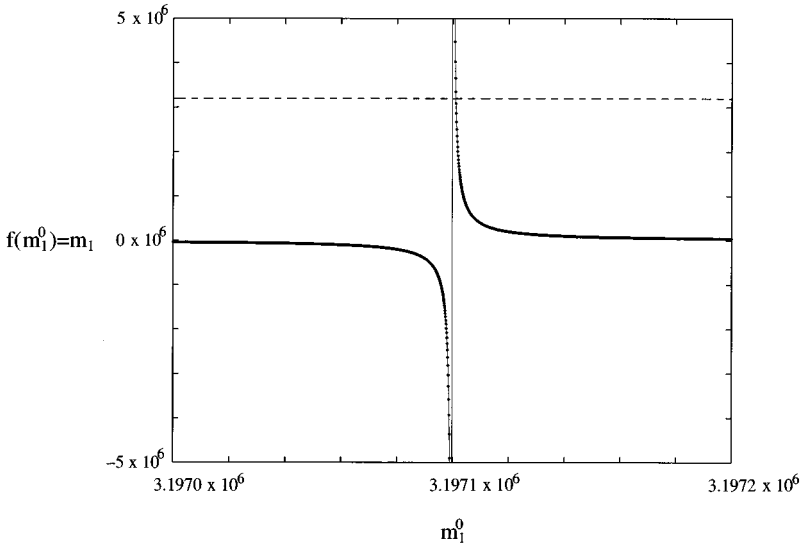

FIG. 1. The function $f(m_1^0)=m_1$, depicted by the plotted points, shows an apparent discontinuity, and a regime in which the bisection algorithm could produce negative solutions. Because the iteration procedure gives rise to discrete values of $f(m_1^0)=m_1$, it is difficult to be sure as to whether the function is actually continuous. If a small enough range of initial values of m_1^0 is iterated over, it becomes apparent that for some parameters the function is actually continuous and that there is no asymptote. This continuous function is indicated by the lightly drawn solid line. The dashed line is the function $f(m_1^0)=m_1^0$.

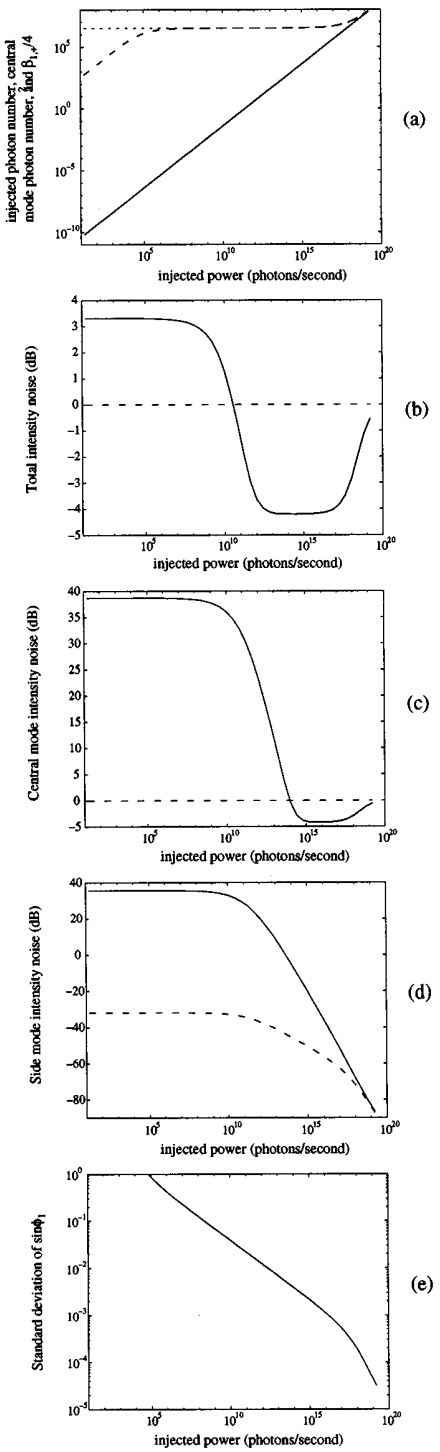

FIG. 2. (a) Injected photon number (solid line), central mode photon number (dotted line), and $\beta_{1,+}^2/4 = m_1 \cos^2\phi$ (dashed line), as a function of injected power, indicating the regime of injection-locking. (b) Total intensity noise as a function of injected power. The dashed line indicates the shot noise level. (c) Central mode intensity noise as a function of injected power. The dashed line indicates the shot noise level of the central mode intensity, normalized to the total intensity noise. (d) Side mode intensity noise as a function of injected power. The dashed line indicates the shot noise level of the side mode intensity normalized to the total intensity noise. The intensity of the side modes (which is not plotted here) also decreases at the same point as the side mode intensity noise begins to decrease. (e) Standard deviation of $\sin\phi_1$ as a function of injected power.

other SDE's under the approximations we have made, we have included its linearized SDE in the drift and diffusion matrices, since it is required for the phase noise description. However, for the calculations of intensity noise, the SDE for $\beta_{1,-}$ is ignored, and we deal with 8×8 matrices rather than 9×9, where the sixth row and column of $\mathcal{F}(\mathbf{Z}_0)$ and $\mathcal{G}(\mathbf{Z}_0)$ (which are those corresponding to the equation for $\beta_{1,-}$) are deleted, as is the sixth element of the vector $\mathbf{z}$.

IV. STEADY-STATE SOLUTIONS

Steady-state solutions must be found for the system of equations describing injection-locking if the matrices (23) and (24) are to be used to calculate the spectrum. Since the variable $\beta_{1,-}$ does not couple into any of the other equations of the system, its steady-state solution can readily be found from (12). Dropping the noise terms and setting $d(\beta_{1,-})=0$, we obtain

$$0=\left(G_{11}^r(\underline{n})-F_{11}^r(\underline{n})-\frac{\kappa_1}{2}+\widetilde{G}_{11}^r(\underline{n})-\widetilde{F}_{11}^r(\underline{n})\right)\beta_{1,-}\,. \tag{25}$$

The term in the large parentheses is nonzero, so in the steady-state $\beta_{1,-}$ will be zero.

The remainder of the system of equations is given by Eqs. (7) and (10) of this paper, and Eqs. (C31)–(C35) of I, where $l=2,3$ in (C35). Because of the complexity of this system of equations, however, steady-state solutions must be found numerically, using an iterative procedure. This involves making some initial guess for the central mode photon number, and using it to calculate a new value of the central mode photon number.

If the noise terms in the system of equations are dropped, and the left hand sides set to zero, then for $P_e=P_h$, Eqs. (C31)–(C35) of I can be rearranged to give Eqs. (D1)–(D4) and (D7),(D8) of I, and Eqs. (7) and (10) of this paper can be rearranged to give the equation

$$m_1=\frac{4|\epsilon|^2+2a_{11}n_e n_h(\kappa_1+2a_{11}N^2-2a_{11}n_e n_h)}{(\kappa_1+2a_{11}N^2-2a_{11}n_e n_h)^2}. \tag{26}$$

Equations (D1)–(D4) of I use an input value of the central mode photon number, which we call m_1^0, to generate values for n_e, n_h, $\widetilde{n}_e$, and $\widetilde{n}_h$. These values can then be substituted into (26) to generate a new value of the central mode photon number m_1. Thus, for a range of values of m_1^0, m_1 can be said to be a function of m_1^0, $m_1=f(m_1^0)$.

When the calculated value m_1, equals (or becomes close enough to) the input value m_1^0, a solution has been found. Referring to Fig 1, we are finding the point at which the function $f(m_1^0)=m_1$ intersects the line $f(m_1^0)=m_1^0$. The procedure used is similar to the bisection approach used in Appendix D of I, except because of the added complication of the injection-locking, one must take extra care in choosing the boundaries of the interval to be bisected at each step.

The plot of the generated value m_1 versus the input value m_1^0 ahown in Fig. 1 illustrates this point. The plot shows that $m_1=f(m_1^0)$ can be negative for some values of m_1^0. In addi-

ion it appears that $m_1 = f(m_1^0)$ is discontinuous. However, careful magnification of $m_1 = f(m_1^0)$ reveals that the function is in fact continuous for some choices of parameters (notably, high injection powers). This continuity gives rise to two possible solutions; however, the solutions which give rise to positive values of the eigenvalues of the drift matrix (in other words, stable solutions) lie on the part of the curve $f(m_1^0)$ with negative slope.

We must be careful to consider these two properties of the function and shift boundaries accordingly. It is important that in finding solutions for m_1, we do not inadvertently shift the boundaries so that our bisection interval spans only negative solutions, or the regime of positive solutions where the slope of $f(m_1^0)$ is positive (in which an unstable solution lies), but which lies beyond (to the left of) the stable solution.

The way in which we choose new upper and lower boundaries therefore differs from that used in the previous case. The first thing to check is whether the value of $m_1 = f(m_1^0)$ obtained is negative. If so, then we shift the lower boundary upwards and rebisect the interval until a positive $m_1 = f(m_1^0)$ is obtained. Second, given that we have a positive value of $m_1 = f(m_1^0)$, we need to check the slope in the region of m_1. If it is positive, then we can shift the lower boundary to this point. If we have a positive solution for m_1, and are on the strictly decreasing portion of the curve, then we use the same procedure as in I. Introducing these extra features was found to have no perceptible effect on the running time of the program.

V. RESULTS

The variances of the individual and total intensity fluctuations, given by Eqs. (19) and (21) of I were calculated, where in this case, the matrices $\mathcal{C}(\mathbf{Y}_0)$ and $\mathcal{E}(\mathbf{Y}_0)$ appearing in Eqs. (20) and (22) of I are replaced with $\mathcal{F}(\mathbf{Z}_0)$ and $\mathcal{G}(\mathbf{Z}_0)$ [Eqs. (23) and (24), where the sixth column and row are ignored], and the intensity fluctuations in the individual modes are normalized with respect to the total shot noise rather than the individual shot noises. Results were obtained for the total, central, and side mode spectrum as a function of injection strength. The values of the decay constants used were $\kappa_1 = \kappa_2 = \kappa_3 = 2.45 \times 10^{11}\ \mathrm{s}^{-1}$, which corresponds to the free-running laser when $\epsilon = 0$. All other parameter sizes are exactly the same as those used in I.

Before we give the spectral results, we first examine the photon number, the injected photon number, and the variation of the phase of the central mode. Referring to Fig. 2(a), the injected photon number, the central mode photon number, and $\beta_{1,+}^2/4$ are plotted as a function of the injection power. Since $\beta_{1,+}^2/4$ can be shown to be $m_1 \cos^2\phi_1$, a plot of $\beta_{1,+}^2/4$ when compared with the value of m_1 gives a measure of the phase ϕ_1. When $\cos\phi_1 = 1$, $\beta_{1,+}^2/4 = m_1$ and phase locking has occurred (since we take the phase of the injected signal to be zero). It can be seen that $\beta_{1,+}^2/4$ approaches the central mode photon number for an injection power of about 10^7. Thus at this point, phase locking has occured, and we expect to begin to see any effects on the spectra due to injection locking.

The injected photon number becomes equal to the central mode photon number for an injection power of about 10^{19}. At this point the injection signal is so strong that it dominates any lasing processes occuring in the cavity, so essentially, all we see is the bare injected signal. In fact, the dominance of the injected signal can be seen in the sudden increase in m_1 for injection powers greater than about 10^{16}. Thus it would be undesirable to work in this regime. The region of interest in terms of seeing effects of injection-locking on the spectra is therefore between injection powers of 10^7 and about 10^{16}.

The intensity spectra are shown in Figs. 2(b)–(d). It can be seen in all three figures that a reduction in the noise occurs as injection power is increased beyond 10^7, the point at which locking occurs. The increase in noise for higher injection strengths is due to the injection power beginning to dominate the system , and thus beyond injection powers of about 10^{16} or 10^{17} the system becomes rather uninteresting. In the regime of interest, the reduction of the noise with increasing injection strength seen in each case, agrees with the results of the Langevin approach of Marin *et al.* The graphs indicate a regime in which there is squeezing in the total intensity, but the side and central modes are unsqueezed, which has been observed experimentally by Marin *et al.*, and a regime in which true single-mode squeezing occurs. Due to technical problems arising at higher injection powers, this single-mode squeezing has not been seen in this system to date. The spectra, which are all normalized with respect to the total noise in the system show particularly well the noise cancellation due to anticorrelated fluctuations. Thus, the intensity noises of the individual modes are almost the same, and their difference gives the total noise which is very small.

In calculating the phase noise, the real quantity of interest is the standard deviation of $\sin\phi_1$. If this is less than 1, we know that the phase is defined to within a revolution. The standard deviation is calculated from the variance as follows,

$$\sqrt{\langle \sin\phi_1(0), \sin\phi_1(0) \rangle} = \sqrt{\frac{1}{2\pi}\int_{-\infty}^{\infty} S_{6,6}(\omega)\, d\omega}$$

$$= \sqrt{\frac{1}{\pi}\int_0^{\infty} \frac{[\mathcal{F}\{(\mathbf{Z}_0) + i\omega\}^{-1}\mathcal{G}(\mathbf{Z}_0)\{\mathcal{F}^T(\mathbf{Z}_0) - i\omega\}^{-1}]_{6,6}\, d\omega}{(\beta_{1,+})^2 + (\beta_{1,-})^2}} \tag{27}$$

where $S_{6,6}(\omega)$ is the spectrum of the correlation function $\langle \sin\phi_1(t), \sin\phi_1(0) \rangle$. The standard deviation is plotted in Fig 2(e). The axes have been chosen so that standard deviations greater than one do not appear, since this means that the phase is random. It can be seen that the standard deviation decreases steadily as locking is achieved. Beyond a locking strength of 10^{16}, the phase noise is extremely small, corresponding to the dominance of the injected signal. For injection powers lower than 10^5, there is no locking, and the fluctuations in the phase are too large for our linearized analysis to be valid.

VI. CONCLUSION

We have adapted the master-equation approach for the multimode semiconductor laser to the case of an injection-locked laser and examined the intensity and phase spectra. We find that the injection-locking causes a decrease in the noise for both the intensity and phase spectra, and that in principle, either true single-mode squeezing, or squeezing only in the total intensity are obtainable. The type of squeezing which is obtained depends on the injected power.

ACKNOWLEDGMENTS

We acknowledge stimulating and interesting discussions with Jean-Philippe Poizat, Helmut Ritsch, and Klaus Gheri. This work was supported by the Marsden Fund under Grant Nos. UOW-306 and GDN-306.

[1] F. Marin *et al.*, Phys. Rev. Lett. **75**, 4606 (1995).
[2] A. Eschmann and C. W. Gardiner, Phys. Rev. A **54**, 760 (1996).
[3] C. W. Gardiner and A. Eschmann, Phys. Rev. A **51**, 4982 (1995).
[4] C. W. Gardiner, *Quantum Noise* (Springer-Verlag, Heidelberg, 1991).